coatings

MDPI

Article

Mn-Doped Glass–Ceramic Bioactive (Mn-BG) Thin Film to Selectively Enhance the Bioactivity of Electrospun Fibrous Polymeric Scaffolds

Mariangela Curcio [1], Brigida Bochicchio [1], Antonietta Pepe [1], Antonio Laezza [1], Adriana De Stefanis [2], Julietta V. Rau [3,4], Roberto Teghil [1] and Angela De Bonis [1,*]

[1] Dipartimento di Scienze, University of Basilicata, Viale dell'Ateneo Lucano, 10, 85100 Potenza, Italy
[2] Istituto di Struttura della Materia, Consiglio Nazionale delle Ricerche (ISM-CNR), Montelibretti Unit, Via Salaria Km 29.300, 00015 Monterotondo Scalo, Italy
[3] Istituto di Struttura della Materia, Consiglio Nazionale delle Ricerche (ISM-CNR), Via del Fosso del Cavaliere 100, 00133 Rome, Italy
[4] Department of Analytical, Physical and Colloid Chemistry, Institute of Pharmacy, Sechenov First Moscow State Medical University, Trubetskaya 8, Build. 2, 119991 Moscow, Russia
* Correspondence: angela.debonis@unibas.it

Abstract: In recent years, significant progress has been made in the development of new technologies to meet the demand for engineered interfaces with appropriate properties for osteochondral unit repair and regeneration. In this context, we combined two methodologies that have emerged as powerful approaches for tissue engineering application: electrospinning to fabricate a nanofibrous polymeric scaffold and pulsed laser deposition to tune and control the composition and morphology of the scaffold surface. A multi-component scaffold composed of synthetic and natural polymers was proposed to combine the biocompatibility and suitable mechanical properties of poly(D,L-lactic acid) with the hydrophilicity and cellular affinity of gelatin. As part of a biomimetic strategy for the generation of bi-functional scaffolds, we coated the electrospun fibers with a thin film of a bioactive glass–ceramic material supplemented with manganese ions. The physico-chemical properties and composition of the bi-layered scaffold were investigated, and its bioactivity, in terms of induced mineralization, was tested by incubation in a simulated body fluid buffer. The processes of the inorganic film dissolution and the calcium phosphate phases growth were followed by microscopic and spectroscopic techniques, confirming that a combination of bioactive glass–ceramics and nanofibrous scaffolds has promising potential in the regeneration of osteochondral tissue due to its ability to induce mineralization in connective tissues.

Keywords: polymeric fibrous scaffold; pulsed laser deposition; bioactive glass; thin films; bioactivity; simulated body fluid (SBF)

Citation: Curcio, M.; Bochicchio, B.; Pepe, A.; Laezza, A.; De Stefanis, A.; Rau, J.V.; Teghil, R.; De Bonis, A. Mn-Doped Glass–Ceramic Bioactive (Mn-BG) Thin Film to Selectively Enhance the Bioactivity of Electrospun Fibrous Polymeric Scaffolds. *Coatings* **2022**, *12*, 1427. https://doi.org/10.3390/coatings12101427

Academic Editor: Charles C. Sorrell

Received: 31 August 2022
Accepted: 27 September 2022
Published: 29 September 2022

1. Introduction

Osteochondral injury is a controversial lesion because it extends across two different tissues (cartilage and bone) connected by a thin interface layer. Due to the increasing of life expectation, one of the most common cartilage disorders is osteoarthritis, a disorder affecting the whole joint in which the potential alteration of the subchondral bone plays a key role in the pathogenesis [1]. The repair of osteochondral tissue is still a big challenge since it is necessary to repair tissues with dissimilar physiological functions and mechanical properties, simultaneously. Moreover, cartilage and bone tissues have different regeneration characteristics; in fact, cartilage, unlike the subchondral bone, is an avascular tissue that is hard to undergo self-healing due to its low cell density and metabolic activity [2].

Significant efforts have been made in the development of strategies for the treatment of osteochondral defects, such as arthroscopic debridement, osteochondral grafting and

chondrocyte implantation, but all these techniques have important limits [3]. The regenerative medicine approach proposes the preparation of scaffolds with a multiphasic or gradient architecture that mimics the complex structure of the osteochondral units [4,5]. The aim is to create a porous structure that not only mimics the inorganic and organic characteristics of the native tissue, acting as a suitable environment for cell adhesion, migration and proliferation, but that is also able to graft the bone, thanks to its osteoconductive properties [6].

A scaffold for cartilage tissue engineering should be biocompatible and biodegradable and should promote the adhesion, migration and proliferation of chondrogenic cells [4]. On the other hand, it should have biomechanical properties suitable for integration with both cartilage and bone. The most promising approach considers a polymeric matrix enriched with bioactive ions and/or molecules that can improve mechanical and tissue interaction characteristics [4,6,7]. Synthetic and natural polymers, such as polypeptide, polysaccharide and polyesters, have been proposed, often in the form of electrospun scaffolds, to ensure a porous structure that provides an appropriate environment for cells attachment and proliferation [8–10]. To improve the interaction with the biological medium in physiological conditions, the polymeric scaffold can be enriched with inorganic materials with osteoconductivity, bioactivity and antimicrobial activity, if possible. Bioactive glasses or glass ceramics can be synthesized to fulfill all these requirements. Since the first bioglass® was proposed [11], many formulations have been prepared, and their biological activity has been tested [12]. Properly selected ions with specific biological activity are usually added to the bioactive matrix to enhance its biological performances. Whereas bioactive glasses have amorphous structure and thermal properties comparable to traditional glasses, glass–ceramic bioactive materials are composed of a silicate network incorporating micro and nanocrystalline phases, mainly apatites. Recently, bioceramics supplemented with functional ions, such as copper, strontium, cobalt and iron, were prepared to tune the properties of the bioactive inorganic material [13]. Among bioactive ions, manganese ions have attracted the interest of the scientific community due to many beneficial effects of manganese on bone growth, defense against reactive oxygen species (ROS), blood coagulation and so on.

Different scaffold architectures have been proposed to combine resorbable scaffolds with bioactive inorganic materials [14,15]. In the most usual approaches, bioactive particles or fibers are mixed with the polymers, acting as filler or deposited as coating to prepare the desired scaffold. To date, many coating techniques have been used to deposit thin bioactive glass films, including mechanical, physical, chemical and biological methods [16]. Herein, we used the nanosecond pulsed laser deposition (PLD) technique since by PLD it is possible to vary different experimental parameters, such as laser wavelength and pulse duration, substrate temperature and deposition environment, allowing the deposition of films with controllable morphology, crystallinity and composition. [17]. Moreover, it has been shown that by PLD, it is possible to deposit thin films characterized by high bonding strength between coating and substrate and micro-nano roughness. All these parameters are important for the cytocompatibility and the in vivo osteointegration of the implant.

The main novelty of this work is the development of a bi-functional polymeric scaffold coated on the inner layer by a Mn supplemented glass–ceramic thin film. The scaffold is composed of a blend of a synthetic polymer (poly(D,L-lactic acid) (PDLLA)) and a natural one (gelatin (GE)). PDLLA is commonly used for producing scaffold employed in bone tissue engineering due to its biocompatibility, bioresorbability and biodegradability properties [10], whereas GE has the ability to promote cell adhesion and increase the hydrophilicity of the scaffold itself [14]. The inner surface of the electrospun scaffold was coated by a thin film of bioceramic material, whose adipogenic, chondrogenic, osteogenic and antimicrobial properties have recently been proved [18].

The micro-nano structured bi-functional scaffold proposed here has a porous structure, and its inner layer has improved bioactivity to support bone growth.

2. Materials and Methods

2.1. Electrospun Scaffold Preparation

GE from bovine skin (type B powder) was purchased from Sigma-Aldrich (St. Louis, MO, USA). PDLLA (EasyFil PLA, transparent pellets, molecular weight: 126,000 g/mol, density: 1240 kg/m^3) was obtained from FormFutura (Nijmegen, The Netherlands).

GE (90 mg) was solubilized in 3 mL of 1,1,1,3,3,3,-hexafluoro-2-propanol (HFIP)at 37 °C and the solution was kept under magnetic stirring for 2 h. Afterward, 270 mg of PDLLA was added and the mixture was kept under magnetic stirring for 3 h. The polymeric blend was loaded into a 5 mL glass syringe with an 18 G stainless-steel needle and then electrospun at 19 kV (Gamma High- Voltage generator) at a flow rate of 1.6 mL/h of the pump BSP-99 mM (Linari Engineering, Pisa, Italy). The plane collector was a round copper plate, having a 90 mm diameter coated with aluminum foil, and the distance between the collector and the needle was set to 19 cm. The scaffold was crosslinked following previously reported procedures [19].

2.2. Mn-BG Synthesis

A bioactive glass material was prepared in the following way: TEOS (tetraethyl orthosilicate), $(P(OEt)_3$, $(Ca(NO_3)_2 \cdot 4H_2O$, $NaNO_3$, $Mg(NO_3)_2 \cdot 6H_2O$, NH_4F, $Mn(NO_3)_2 \cdot 4H_2O$ and KNO_3 were added, in this order, one after another, at intervals of 30 min, to a 0.1 M solution of HNO_3. Nitric acid was needed for the hydrolysis TEOS and $(P(OEt)_3$. All components were kept in a Teflon bottle under stirring until complete homogenization of the colloidal solution. This sol was then left to evolve for 10 days and subsequently treated at 70 °C for 72 h. The recovered gel was dried and, for this purpose, underwent heating at 120 °C for 48 h. In this way, the sol-gel granules were produced following another thermal treatment at 700 °C in air. Pellets of 1 cm of diameter and 0.4 cm of thickness were prepared by grinding the granules to powder, which was then pressed at 500 MPa for 5 min and finally sintered at 1100 °C in air.

The final composition was: SiO_2 [37.5], P_2O_5 [7.43], CaO [40.7], Na_2O [2.00], MgO [2.49], CaF_2 [8.74], K_2O [0.06], MnO [1.08] ([wt %] in parentheses). The material was named Mn-BG, and some of its properties were previously described by us in [18,20,21].

2.3. Thin Film Deposition

A Nd:YAG pulsed laser source (λ: 532 nm, τ: 10 ns, repetition rate: 10 Hz, fluence: 12 J·cm^{-2}) was used for all depositions. The laser beam was focused on the target surface with an inclination of 45° by means of a quartz lens (f = 350 mm). All depositions were carried out in a vacuum chamber at working pressure of 10^{-4} Pa and at room temperature. The chamber was equipped with a rotating holder for the target, in order to minimize the laser induced craterization effect. Monocrystalline silicon (Si (100) Goodfellow) was used as a substrate for X-ray Diffraction (XRD) and Fourier Transform Infrared (FTIR) characterization of the deposited coatings, whereas films deposited onto polymeric scaffold substrates were used for the bioactivity test. The deposition conditions were previously optimized for a deposition time of 4 h, with a substrate-target distance of 2 cm. The mean thickness of the deposited films, evaluated by SEM analysis of films deposited on silicon substrates, was 300 nm.

2.4. Materials Characterization

XRD analysis was carried out by using a Siemens 5000 X-ray diffractometer (Siemens, Munich, Germany) operating at 40 kV and 32 mA. The explored range was from 20 2θ° to 60 2θ° at a step of 0.04°, using CuKα radiation (wavelength of 1.5406 Å).

FT-IR analysis was performed by using a Jasco FT-IR 460 Plus interferometer (Jasco, Halifax, Canada). Films deposited onto silicon substrates were analyzed in transmittance mode, the spectra were acquired by collecting 100 scans at 4 cm^{-1} resolution, in the range of 4000–400 cm^{-1}. Attenuated Total Reflectance (ATR) configuration was used to acquire vibrational spectra of scaffolds before and after their soaking in SBF solution.

The morphology of the deposited film was studied by means of scanning electron microscopy (SEM). SEM images were acquired by (PHILIPS-FEI XL30, North Billerica, MA, USA), coupled with an X-ray Energy Dispersive Spectroscopy (X-EDS) system for microanalysis.

The surface composition of the films was characterized with the use of X-ray photoelectron spectroscopy (XPS, Leybold, Cologne, Germany, LH-Leybold X1 spectrometer equipped with a polychromatic Mg Kα radiation and operating at a constant power of 260 W). Wide and detailed spectra were acquired with a resolution of 1 and 0.1 eV, respectively. Peak positions were referenced to the C1s aliphatic carbon set at 285.0 eV, and peak areas were evaluated considering their sensitivity factor.

To investigate the bioactivity in vitro, the protocol proposed by Kokubo et al. was followed [22]. For the preparation of the simulated body fluid (SBF), the chemicals (purchased from the Carlo Erba, Milan, Italy) were dissolved in bi-distilled milli-Q water in the following order: NaCl (100.5%, 7.9550 g), $NaHCO_3$ (100.0%, 0.3532 g), KCl (100.5%, 0.2228 g), $K_2HPO_4 \cdot 3H_2O$ (100.0%, 0.2287 g), $MgCl_2 \cdot 6H_2O$ (99.0%, 0.2988 g), HCl 1 M (39 mL), $CaCl_2 \cdot 2H_2O$ (100.5%, 0.2760 g), Na_2SO_4 (100.0%. 0.0713 g), and tris-(hydroxymethyl) aminomethane (TRIS) (99.5%, 6.0873 g). The pH was adjusted at 7.40 exactly at 36.5 °C with HCl 1 M. For this purpose, coated scaffolds were placed in a plastic tube and submerged in SBF. The proper volume of SBF was calculated according to the formula $V_{SBF} = Sa/10$, where V_{SBF} is the volume of SBF (mL) and Sa is the apparent surface area of the sample (mm^2) [22]. The tubes were kept at 37 °C, and SBF was changed twice a week. XRD, ATR-FTIR spectroscopy and SEM-EDX analyses were performed to assess the formation of calcium phosphate phases on the coatings.

3. Results and Discussion

3.1. Mn-BG Film Characterization

3.1.1. Morphological Characterization

Mn-BG films deposited on smooth substrates (monocrystalline Si) are dense, uniform and present a compact background overlaid by sub-micrometric and micrometric fused particles, as reported for ceramic films deposited by nanosecond PLD, usually [17]. In Figure 1, SEM images of Mn-BG film deposited on the surface of the polymeric scaffold are presented. The fibers of the scaffold exposed to the laser induced plasma are fully covered by a compact background with a nanometric morphology formed by particles ejected or condensed in the plasma plume or on the landing surface. Spherical microparticles adhere to the fibers, and large particles with a smooth top flat surface suggest that droplets were ejected during the ablation process. The fibers of the scaffold face not exposed to the laser induced plasma retained their smooth morphology, confirming that a system with two different functionalities was obtained (Figure 1d).

3.1.2. XRD and FT-IR Characterization

Bioactive glasses are formed by some crystalline phases embedded in an amorphous matrix, usually [12,18]. XRD analysis of the Mn-BG target allows to recognize some crystalline peaks that can be assigned to cristobalite (JPCD: 00-003-0270), wollastonite (JPCD: 00-027-0088) and fluorapatite (JPCD: 01-079-1459) phases. Mn-BG film deposited by PLD at room temperature partially loses its crystalline structure and its XRD spectrum shows low intensity signals superimposed on a broad background. The two main peaks observed at 30° and 31° in Figure 2 can be assigned to the wollastonite and fluorapatite phases, respectively.

The FTIR spectrum of the Mn-BG target is dominated by the broad bands of the silicate component. The bands centered at 474 and 1040 cm^{-1} are related to the Si-O-Si bending and stretching modes respectively, whereas the band centered at 930cm^{-1} is related to Si-O oxygen bonds in non bridging bonds configuration [23]. The phosphate group contributes with the bands 602, 930 and 1090 cm^{-1}, where the narrow signal at 602 cm^{-1} suggests the presence of crystalline apatite phases [24].

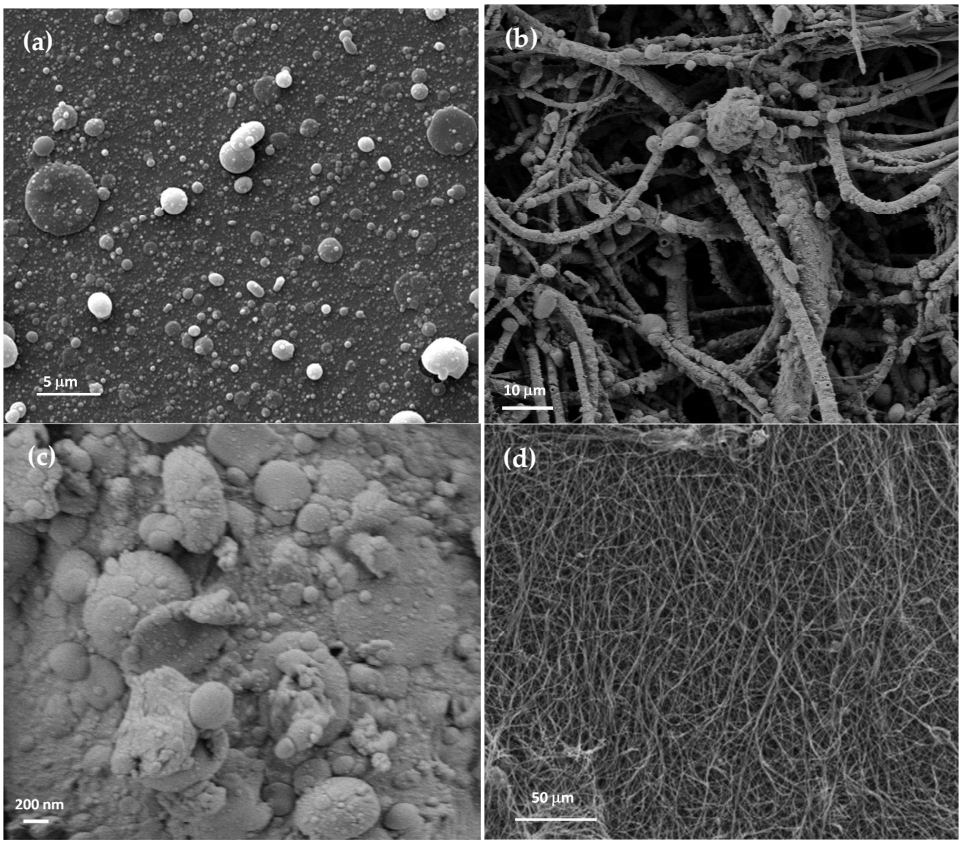

Figure 1. (**a**) SEM image of the Mn-BG coating deposited on silicon substrate. (**b**,**c**) SEM images of the Mn-BG coating deposited on the polymeric scaffold at two different magnification (**b**) 2500×, (**c**) 50,000×. (**d**) SEM image of the surface of the scaffold not exposed to the laser induced plasma.

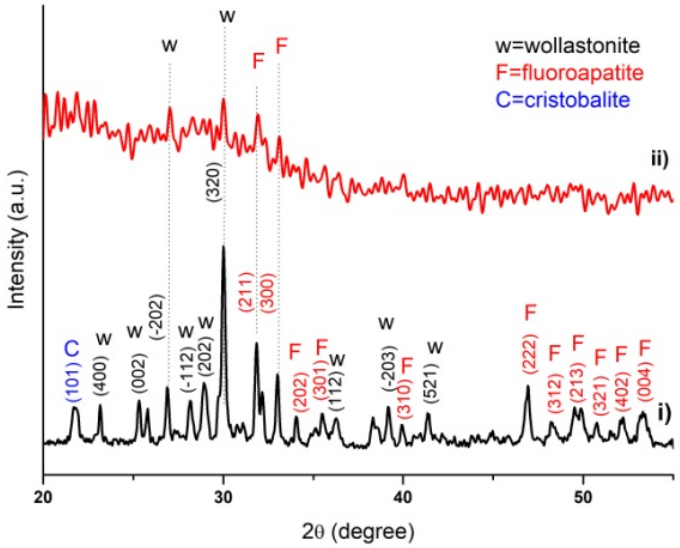

Figure 2. XRD spectra of the Mn-BG target (i) (black line) and of the Mn-BG film deposited on silicon substrate (ii) (red line).

The spectrum in Figure 3a suggests that the film deposited on the silicon substrate retains the target composition. The vibrational bands of silicate and phosphate are present, with the exception of the 602 cm^{-1} peak, confirming the lower crystallinity of films obtained by PLD with respect to the target. Vibrational analysis of the polymeric scaffolds was performed in ATR configuration. The ATR-FTIR spectrum of the scaffold (Figure 3b)

exhibits the typical absorption bands of GE and PDLLA components. The amide I and amide II bands, at 1645 and 1551 cm^{-1}, respectively, are hallmarks of the protein component. The characteristic features of PDLLA are the aliphatic C−H stretching bands at 2948 and 2997 cm^{-1}, the ester C=O stretching at 1755 cm^{-1}, the (C=O)-O stretching at 1180 cm^{-1} and the O-C-C stretching band at 1090 cm^{-1} [19]. In the ATR-FTIR spectrum of Mn-BG film deposited on the surface of the polymeric scaffold, it was not possible to recognize the characteristic bands of the bioactive glass, probably due to both the presence of the high intensity signals of the scaffold itself in the same wavelength range and to the low film thickness.

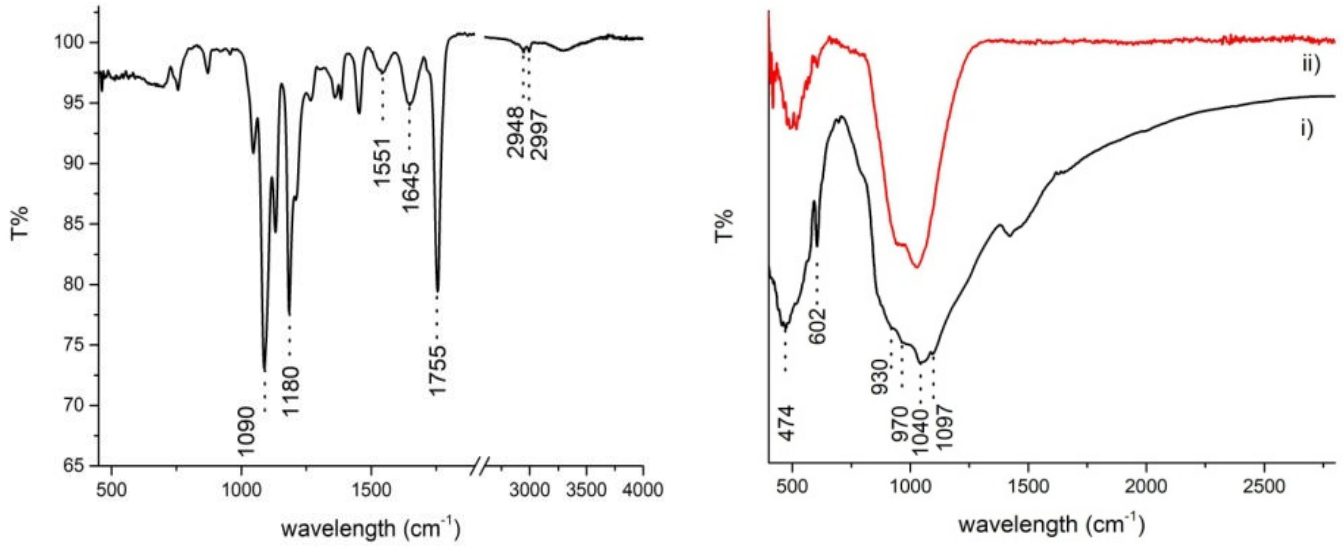

(**a**) (**b**)

Figure 3. (**a**) FTIR spectra of (i) the Mn-BG target (black line), (ii) the Mn-BG film deposited on silicon substrate (red line); (**b**) ATR-FTIR spectrum of the polymeric scaffold.

3.2. In Vitro Bioactivity of the Bi-Functional Mn-BG/Polymeric Scaffold

The bioactivity is the ability of a biomaterial to support the formation of apatite-like phases when it interacts with the biological medium. Bioactivity is one of the most critical requirements for bone repair materials since it can enhance their bone binding competence [8,25]. The biological activity of coatings can be evaluated by observing the formation of bone-like apatite minerals when they are soaked in SBF at a controlled temperature and pH. Depending on its composition and crystallinity, the coating begins to degrade and induces apatite deposition, forming a new morphology and structure on the bioactive surface [26]. The ability to induce the growth of different calcium phosphate phases was evaluated in vitro by soaking the bi-layered scaffolds for periods of 3, 7, 14, and 28 days in the SBF solution. The minerals formation was investigated by the SEM-EDS, ATR-FTIR, XRD and XPS techniques.

3.2.1. Kinetic Study of Film Bioactivity

By XPS spectroscopy, it was possible to characterize the chemical composition of the outermost surface, study the kinetics of dissolution of the bioactive glass film and describe the growth of the apatite-like phases on the coated surface of the bi-layered scaffold. The XPS spectra of Ca2p and P2p-Si2p regions obtained at 0, 3, 14 and 28 days of soaking in SBF solution are reported in Figure 4.

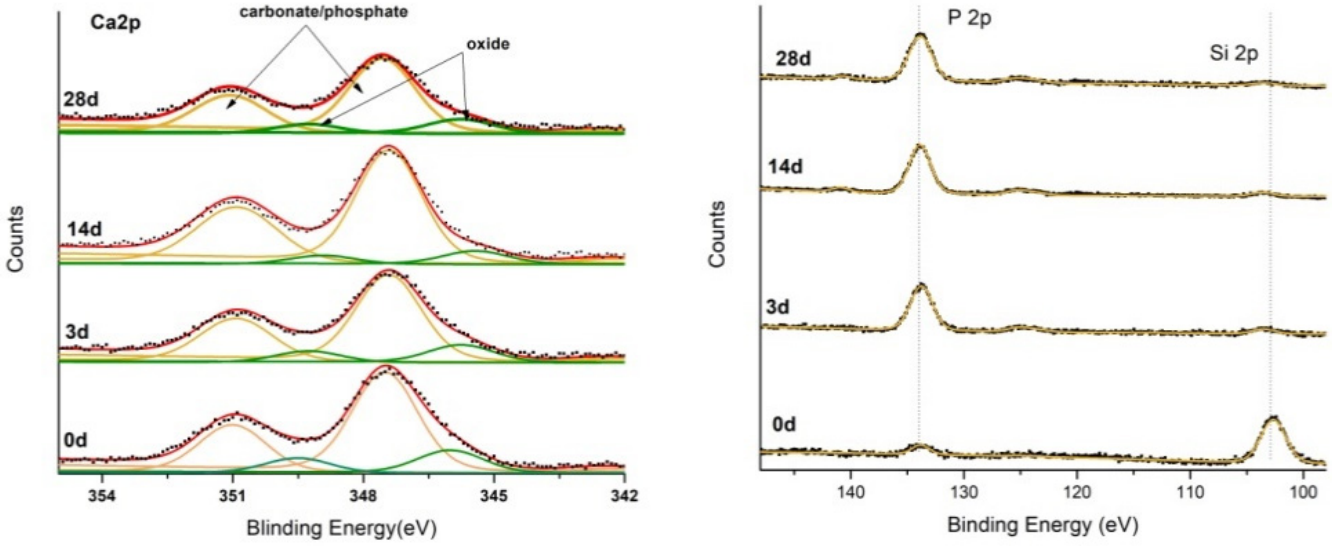

(**a**) (**b**)

Figure 4. XPS spectra of the coated polymeric scaffold at different soaking time in SBF solution: 0 (0d), 3 (3d), 14 (14d) and 28 days (28d). (**a**) Ca2p region; (**b**) P2p-Si2p region.

Irrespective of the soaking time, the Ca2p signal can be resolved with two doublets: the doublet at Binging Energy (B.E.) of 347.5 and 351 eV can be assigned to Ca2p3/2 and Ca2p1/2 of Ca^{2+} ions bonded to phosphate and/or carbonate ions [27,28], and the doublet at B.E. of 345.9 and 349.5 eV can be assigned to Ca2p3/2 and Ca2p1/2 of Ca bonded to oxygen in calcium oxide [29]. In the 90–150 eV range, the signals of P2p and Si2p can be observed. The P2p peak is centered at B.E. of 133.4 eV and can be related to phosphorus in a phosphate environment [28]. The Si2p signal is centered at B.E. of 103.1 eV and can be related to silicon atoms bonded to oxygen in siloxane groups [29]. The Ca/P ratio evaluated for the as deposited film is about 7, suggesting that a certain amount of calcium carbonate phase is present on the outermost surface of the coating. The formation of calcium carbonate has been already reported for films deposited by the PLD technique [30]. Whereas the peaks positions remain almost unchanged, a decrease in the Si2p contribution and an increase in the P2p contribution were observed with increasing the soaking time in SBF solution. The Ca/Si ratio increases from 0.8 for the as deposited film to 7.2 and 10.7 after 3 and 28 days of SBF soaking, respectively. The quick decrease in the Si2p signal can be understood considering that during the soaking time, the dissolution of the Mn-BG coating occurs, confirming the fast release kinetics of silicon ions already reported for glass ceramic composite soaked in SBF [18]. At the same time, the ions released in the SBF solution by the bioactive film support the rapid growth of a calcium phosphate layer on the outermost surface, and after 28 days of soaking, the Ca/P ratio reaches a value of 1.2 (Figure 5).

3.2.2. Morphological Characterization

The quick dissolution of the film was confirmed by SEM-EDS analysis. In Figure 6, the SEM images of Mn-BG coated scaffolds after 7, 14 and 28 days of soaking in SBF solution are reported. After 7 days the dissolution of Mn-BG film and the formation of irregular structures are clearly visible. EDS analysis confirms that the new structures are composed mainly of calcium and phosphorus with an average Ca/P ratio of 2.2, due to the formation of Ca rich amorphous calcium phosphate species in the early soaking period [31]. With increasing the soaking time, a fine-grained structure grows on the surface of the fibers, and the Ca/P ratio reaches an average value of 1.6, very close to the expected ratio for hydroxyapatite-like phases. After 28 days of soaking, all the fibers are completely covered by a newly formed apatite-like layer. The densely packed layer grown on the fibers surface is formed by the coalescence of nanometric particles.

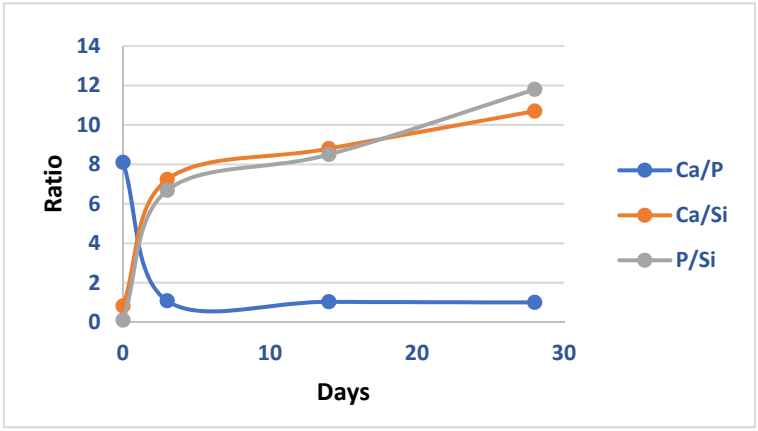

Figure 5. Ca/P, Ca/Si, P/Si ratios at different time of SBF soaking (0, 3, 14 and 28 days) evaluated by XPS analysis.

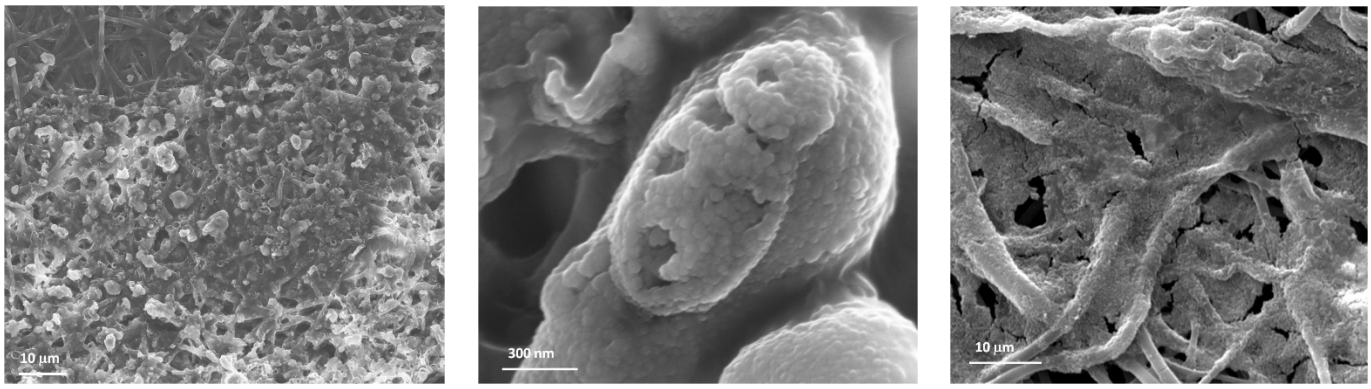

(**a**) (**b**) (**c**)

Figure 6. SEM images of the coated polymeric scaffold at different times of soaking in SBF (**a**) 7 days; (**b**) 14 days; (**c**) 28 days.

The ATR-FTIR spectra registered for the hybrid scaffolds at different immersion times in the SBF solution are reported in Figure 7. All spectra were normalized with respect to the signal centered at 1760 cm^{-1} that can be related to the C=O stretching of PDLLA [19]. By increasing the soaking time, the appearance of the typical phosphate vibrational signals can be observed. After 14 days, a broad band centered at about 570 cm^{-1} and the broadening of the band centered at 1049 cm^{-1} can be appreciated. After 28 days a broad band at 480 cm^{-1} and two signals at 574 and 603 cm^{-1} are clearly visible. These peaks can be assigned to ν_2 and ν_4 modes of PO_4^{3-} group, respectively. The ν_1 and ν_3 modes of the phosphate group are in the 900–1200 cm^{-1} range, at the same wavelength where the high intensity signals of the –C-O-C functionality of the polymeric scaffold is present [32]. We may expect that the growth of the apatite layer could be at the origin of the broadening and increase in intensity of the bands in this region. However, the calcium phosphate signals are broad, suggesting the presence of different low crystalline phases.

3.2.3. ATR-IR and XRD Characterization

According to SEM and ATR-IR data, the signature of HA crystalline phase at $2\theta = 32°$, corresponding to the (112) reflection plane of HA, is visible after 28 days of soaking (Figure 8). The broad and low intensity peak of the HA phase suggests that non-stoichiometric and/or nanoscale size new apatite crystals are grown on the surface of the Mn-BG-coated polymeric scaffold.

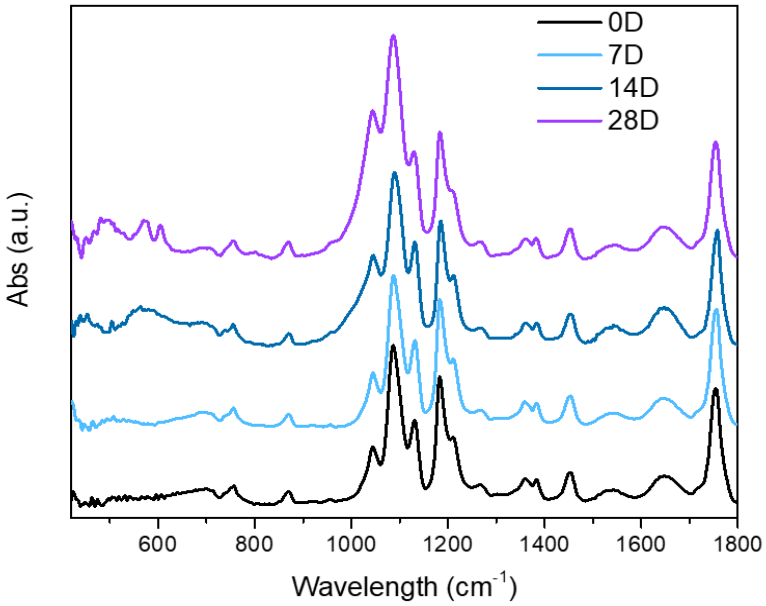

Figure 7. ATR-FTIR analysis of the coated polymeric scaffold at different time of soaking in SBF (0 (0D), 3 (3D), 14 (14D) and 28 days (28D)).

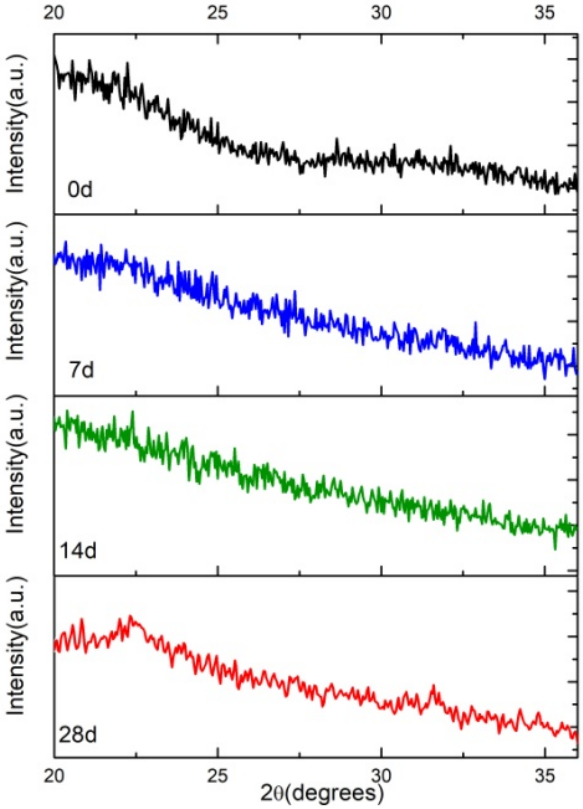

Figure 8. XRD analysis of the coated polymeric scaffold at different time of soaking in SBF: 0 (0D), 3 (3D), 14 (14D) and 28 days (28D).

It should be noted that none of the apatite features can be recognized on the uncoated polymeric surface, either by XRD and ATR-FTIR measurements. The uncoated surface of the scaffold is composed of smooth fibers, without any signs of degradation.

Based on the obtained results, it can be concluded that the prepared biphasic scaffold presents the suitable properties for the repair and regeneration of the calcified cartilage tissue. The two different regions resemble the stratified anatomical architecture of the

osteochondral unit in which the articular cartilage and the subchondral bone coexist, and the bi-functional scaffold provides an appropriate environment for the restoration of the complex tissue. The porous structure provides a skeleton for the cell attachment, and the gradient interface could allow the integration with both the cartilage and the bone tissues.

4. Conclusions

In this study, we prepared an organic–inorganic fibrous scaffold combining electrospinning and pulsed laser deposition techniques. The electrospun polymeric matrix (PDLLA/GE) was coated on the inner surface with a glass ceramic layer (Mn-BG). The deposited film, formed by the coalescence of micro and nanoparticles, retained the target composition and fully covered the polymeric surface exposed to the laser-induced plasma. The bioactivity of the bi-layered scaffold was tested by soaking it in a SBF solution. The analysis of the outermost surface of the bi-layered scaffold highlights that the Ca/Si ratio increased from 0.8 for the as-deposited film to 7.2 after three days of soaking, suggesting the rapid dissolution of the bioactive glass coating. With increasing soaking time, the Ca/P ratio reached an average value of 1.6 due to the growth of calcium phosphate minerals, as was observed by SEM-EDS analysis. After 28 days of immersion in SBF solution, a densely packed layer of nanocrystalline HA fully covered the scaffold inner surface, whereas the uncoated scaffold surface did not show any evidence of apatite deposition. The bi-functional and depth-dependent organization of the prepared scaffold mimics the transition zone between bone and cartilage, resembling the hierarchical architecture of the osteochondral unit. Due to its biocompatibility characteristics and the ability to induce biomineralization only on the coated surface, it could represent a promising strategy with regard to the restoration of the complex osteochondral tissue.

Author Contributions: Conceptualization: R.T. and A.D.B.; methodology: M.C., B.B., A.P., A.L., A.D.S., J.V.R. and A.D.B.; validation: M.C., A.L., A.D.S., J.V.R., R.T. and A.D.B.; investigation: M.C. and A.D.S.; data curation: M.C. and A.D.B.; writing—original draft preparation: A.D.B.; writing—review and editing: all authors. All authors have read and agreed to the published version of the manuscript.

Funding: This research received no external funding.

Institutional Review Board Statement: Not applicable.

Informed Consent Statement: Not applicable.

Data Availability Statement: Not applicable.

Conflicts of Interest: The authors declare no conflict of interest.

References

1. Mendes, L.F.; Bosmans, K.; Van Hoven, I.; Viseu, S.R.; Marèchal, M.; Luyte, F.P. Developmental engineering of living implants for deep osteochondral joint surface defects. *Bone* **2020**, *139*, 115520. [CrossRef] [PubMed]
2. Makris, E.A.; Gomoll, A.H.; Malizos, K.N.; Hu, J.C.; Athanasiou, K.A. Repair and tissue engineering techniques for articular cartilage. *Nat. Rev. Rheumatol.* **2015**, *11*, 21–34. [CrossRef] [PubMed]
3. You, B.; Li, Q.; Dong, H.; Huang, T.; Cao, X.; Liao, H. Bilayered HA/CS/PEGDA hydrogel with good biocompatibility and self-healing property for potential application in osteochondral defect repair. *J. Mater. Sci. Technol.* **2018**, *34*, 1016–1025. [CrossRef]
4. Gao, J.; Ding, X.; Yu, X.; Chen, X.; Zhang, X.; Cui, S.; Shi, J.; Chen, J.; Ding, J. Cell-free bilayered porous scaffolds for osteochondral regeneration fabricated by continuous 3D-printing using nascent physical hydrogel as ink. *Adv. Healthc. Mater.* **2021**, *10*, 2001401. [CrossRef]
5. Wei, W.; Dai, H. Articular cartilage and osteochondral tissue engineering techniques: Recent advances and challenges. *Bioact. Mater.* **2021**, *6*, 4830–4855. [CrossRef]
6. Dargoush, S.A.; Hanaee-Ahvaz, H.; Irani, S.; Soleimani, M.; Khatami, S.M.; Sohi, A.N. A composite bilayer scaffold functionalized for osteochondral tissue regeneration in rat animal model. *J. Tissue Engeneering Regen. Med.* **2022**, *15*, 559–574. [CrossRef]
7. Xiao, Y.; Wang, L.; Luo, K.; Yang, Y.; Zhang, P.; Li, J. 3D biocompatible polyester blend scaffolds containing degradable calcium citrate for bone tissue engineering. *J. Bionic Engeneering* **2022**, *19*, 497–506. [CrossRef]
8. Zou, L.; Zhang, Y.; Liu, X.; Chen, J.; Zhang, Q. Biomimetic mineralization on natural and synthetic polymers to prepare hybrid scaffolds for bone tissue engineering. *Colloids Surf. B Biointerface* **2019**, *178*, 222–229. [CrossRef]

9. Siqueira, L.; Passador, F.R.; Costa, M.M.; Lobo, A.O.; Sousa, E. Influence of the addition of β-TCP on themorphology, thermal properties and cell viability of poly (lactic acid) fibers obtained by electrospinning. *Mater. Sci. Eng. C* **2015**, *52*, 135–143. [CrossRef]
10. Petre, D.G.; Leeuwenburgh, S.C.G. The use of fibers in bone tissue engineering. *Tissue Eng. Part B Rev.* **2022**, *28*, 141–159. [CrossRef]
11. Hench, L.L. Bioceramics: From concept to clinic. *J. Am. Ceram. Soc.* **1991**, *74*, 1487–1510. [CrossRef]
12. Singh, P.; Yu, X.; Kumar, A.; Kumar Dubey, A. Recent advances in silicate-based crystalline bioceramics for orthopedic applications: A review. *J. Mater. Sci.* **2022**, *57*, 13109–13151. [CrossRef]
13. Schatkoski, V.M.; do Amaral Montanheiro, T.L.; Rossi Canuto de Menezes, B.; Monteiro Pereira, R.; Rodrigues, K.F.; Guimaraes Ribas, R.; Morais da Silva, D.; Patrocínio Thim, G. Current advances concerning the most cited metal ions doped bioceramics and silicate-based bioactive glasses for bone tissue engineering. *Ceram. Int.* **2021**, *47*, 2999–3012. [CrossRef]
14. Bochicchio, B.; Barbaro, K.; De Bonis, A.; Rau, J.V.; Pepe, A. Electrospun poly(d,l-lactide)/gelatin/glass-ceramics tricomponent nanofibrous scaffold for bone tissue engineering. *J. Biomed. Mater. Res. Part A* **2020**, *108*, 1064–1076. [CrossRef]
15. Niu, X.; Qin, M.; Xu, M.; Zhao, L.; Wei, Y.; Hu, Y.; Lian, X.; Chen, S.; Chen, W.; Huang, D. Coated electrospun polyamide-6/chitosan scaffold with hydroxyapatite for bone tissue engineering. *Biomed. Mater.* **2021**, *16*, 025014. [CrossRef]
16. Montazerian, M.; Hosseinzadeh, F.; Migneco, C.; Fook, M.V.L.; Baino, F. Bioceramic coatings on metallic implants: An overview. *Ceram. Int.* **2022**, *48*, 8987–9005. [CrossRef]
17. Teghil, R.; Curcio, M.; De Bonis, A. Substituted hydroxyapatite, glass, and glass-ceramic thin films deposited by nanosecond pulsed laser deposition (PLD) for biomedical applications: A systematic review. *Coatings* **2021**, *11*, 811. [CrossRef]
18. Rau, J.V.; De Stefanis, A.; Barbaro, K.; Fosca, M.; Yankova, V.G.; Matassa, R.; Nottola, S.A.; Nawaz, Q.; Saad Ali, M.; Peukert, W.; et al. Adipogenic, chondrogenic, osteogenic, and antimicrobial features of glass ceramic material supplemented with manganese. *J. Non-Cryst. Solids* **2021**, *559*, 120709. [CrossRef]
19. Ciarfaglia, N.; Pepe, A.; Piccirillo, G.; Laezza, A.; Daum, R.; Schenke-Layland, K.; Bochicchio, B. Nanocellulose and elastin act as plasticizers of electrospun bioinspired scaffolds. *ACS Appl. Polym. Mater.* **2020**, *2*, 4836–4847. [CrossRef]
20. Sabino, R.M.; Rau, J.V.; De Bonis, A.; De Stefanis, A.; Curcio, M.; Teghil, R.; Popat, K.C. Manganese-doped bioactive glass enhances osteogenic activity of TiO_2 nanotube arrays. *Appl. Surf. Sci.* **2021**, *570*, 151163. [CrossRef]
21. Cassari, L.; Brun, P.; Di Foggia, M.; Taddei, P.; Zamuner, A.; Pasquato, A.; De Stefanis, A.; Valentini, V.; Saceleanu, V.M.; Rau, J.V.; et al. Mn-containing bioactive glass-ceramics: BMP-2-mimetic peptide covalent grafting boosts human-osteoblast proliferation and mineral deposition. *Materials* **2022**, *15*, 4647. [CrossRef] [PubMed]
22. Kokubo, T.; Takadama, H. How useful is SBF in predicting in vivo bone bioactivity? *Biomaterials* **2006**, *27*, 2907–2915. [CrossRef] [PubMed]
23. Rau, J.V.; De Bonis, A.; Curcio, M.; Schuhladen, K.; Barbaro, K.; De Bellis, G.; Teghil, R.; Boccaccini, A.R. Borate and silicate bioactive glass coatings prepared by nanosecond pulsed laser deposition. *Coatings* **2020**, *10*, 1105. [CrossRef]
24. Nasker, P.; Mukherjee, M.; Kant, S.; Tripathy, S.; Sinha, A.; Das, M. Fluorine substituted nano hydroxyapatite: Synthesis, bio-activity and antibacterial response study. *Ceram. Int.* **2018**, *44*, 22008–22013. [CrossRef]
25. Zhang, P.; Hong, Z.; Yu, T.; Chen, X.; Jing, X. In vivo mineralization and osteogenesis of nanocomposite scaffold of poly(lactide-co-glycolide) and hydroxyapatite surface grafted with poly(L-lactide). *Biomaterials* **2009**, *30*, 58–70. [CrossRef] [PubMed]
26. Yu, Y.; Mathew, R.; Eden, M. Quantitative composition–bioactivity relationships of phosphosilicate glasses: Bearings from the phosphorus content and network polymerization. *J. Non-Cryst. Solids* **2018**, *502*, 106–117. [CrossRef]
27. Zhu, D.; Wang, J.; Hu, W. Hydroxyapatite film prepared by hydrothermal method on layered double hydroxides coated Mg Alloy and its corrosion resistance. *Colloids Surf. A* **2022**, *647*, 129075. [CrossRef]
28. Cao, J.; Lian, R.; Jiang, X. Magnesium and fluoride doped hydroxyapatite coatings grown by pulsed laser deposition for promoting titanium implant cytocompatibility. *Appl. Surf. Sci.* **2020**, *515*, 146069. [CrossRef]
29. de Oliveira, L.G.; Cotta, A.A.; Macedo, W.A.A.; Vasconcellos, W.A.; Ferreira, A.J.; Moreira, A.N.; Barros, V.M.; Domingues, R.Z.; Porto, A.O. Bioglass Ti coatings: Influence of thermal annealing on the evolution of calcium phosphate formation, phase and morphology. *J. Non-Cryst. Solids* **2021**, *576*, 120926. [CrossRef]
30. De Bonis, A.; Uskoković, V.; Barbaro, K.; Fadeeva, I.; Curcio, M.; Imperatori, L.; Teghil, R.; Rau, J.V. Pulsed laser deposition temperature effects on strontium-substituted hydroxyapatite thin films for biomedical implants. *Cell Biol. Toxycology* **2020**, *36*, 537–551. [CrossRef]
31. Milovac, D.; Gallego Ferre, G.; Ivankovic, M.; Ivankovic, H. PCL-coated hydroxyapatite scaffold derived from cuttlefish bone: Morphology, mechanical properties and bioactivity. *Mater. Sci. Eng. C* **2014**, *34*, 437–445. [CrossRef] [PubMed]
32. Ofkeli, F.; Demir, D.; Bolgen, N. Biomimetic mineralization of chitosan/gelatin cryogels and in vivo biocompatibility assessments for bone tissue engineering. *J. Appl. Polym. Sci.* **2021**, *138*, e50337. [CrossRef]